THE JOURNAL OF PHYSICAL CHEMISTRY

Letter

Letters

Cite This: J. Phys. Chem. Lett. 2018, 9, 4275−4281

pubs.acs.org/JPCL

# High-Pressure Methane Adsorption in Porous Lennard-Jones Crystals

Alec R. Kaija and Christopher E. Wilmer*

Department of Chemical & Petroleum Engineering, University of Pittsburgh, 3700 O'Hara Street, Pittsburgh, Pennsylvania 15261, United States

* Supporting Information

ABSTRACT: Decades of research have yet to yield porous adsorbents that meet the U.S. Department of Energy's methane storage targets. To better understand why, we calculated high-pressure methane adsorption in 600 000 randomly generated porous crystals, or "pseudomaterials," using atomistic grand canonical Monte Carlo (GCMC) simulations. These pseudomaterials were periodic configurations of Lennard-Jones spheres whose coordinates in space, along with corresponding well depths and radii, were all chosen at random. GCMC simulations were performed for pressures of 35 and 65 bar at a temperature of 298 K. Methane adsorption was compared for all materials against a range of other properties: average well depths and radii, number density, helium void fraction, and volumetric surface area. The results reveal structure−property relationships that resemble those previously observed for metal−organic frameworks and other porous materials. We contend that our computational methodology can be useful for discovering useful structure−property relationships related to gas adsorption without requiring experimentally accessible structural data.

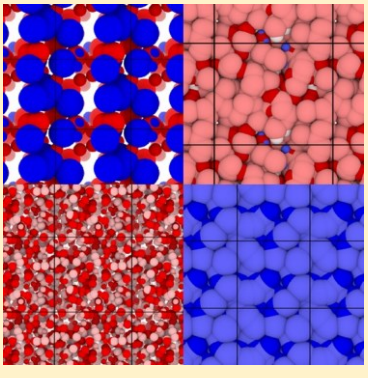



The discovery of tunable, high-surface area, porous materials known as metal−organic frameworks (MOFs)[1] has sparked considerable interest over the past two decades in developing adsorbents for various industrial applications including gas storage and separations,[2−9] catalysis,[10−18] and sensing.[19−26] In particular, the application of high-pressure methane storage has driven significant exploratory efforts in the MOF field. Although tens of thousands of MOFs have been synthesized, there are still potentially millions more that remain undiscovered.[27−32] In addition to experimental efforts, large-scale computational screening has been used extensively on hundreds of thousands of real and hypothetical MOFs and related materials to find promising targets for methane storage.[33−36] In addition to identifying useful targets for synthesis, these large-scale screening studies have contributed significant insights via the discovery of clear structure−property relationships.[37,38] Many researchers have utilized large libraries of hypothetical porous materials (5000 to 600 000 materials) to observe structure−property relationships related to gas adsorption.[39−43]

Despite these efforts, MOFs discovered to date (including the hypothetical ones) have not met the high methane storage targets set by the U.S. Department of Energy (DOE): 315 $cm^3$(STP)/$cm^3$ at 35 or 65 bar and ambient temperature.[44−48] However, given the vast space of possible MOFs, it is not clear whether a performance ceiling has been reached or whether higher performing MOFs await discovery. A higher performing porous material could also be discovered in a different material class altogether (e.g., zeolites).

In addition to libraries of MOFs, there are libraries of hypothetical zeolites,[49,50] porous polymer networks (PPNs),[16,40,41,47,49,51] and zeolitic imidazolate frameworks (ZIFs).[50] In particular, a wide range of porous polymers have recently shown significant promise as $CH_4$ (and also $CO_2$ and $N_2$) adsorbents.[52−56] However, to date, virtually all attempts at creating large libraries of hypothetical porous materials have relied on modular chemical building blocks and design rules inherent to a particular material class. But what if new materials exist that do not obey previously observed design rules or that cannot be constructed from previously studied building blocks? Using these design rules alone to create a comprehensive library of porous materials might result in





DOI: 10.1021/acs.jpclett.8b01421
J. Phys. Chem. Lett. 2018, 9, 4275−4281

holes where new materials might exist. These holes might limit our understanding of the full range of structure−property relationships for porous materials.

In this study, in an attempt to generalize structure−property observations of methane adsorption across disparate material classes, we have generated and studied porous "pseudomaterials", periodic configurations of Lennard-Jones (LJ) spheres meant to represent arbitrary porous crystals. This pseudomaterials approach makes it possible to sample regions of the structure−property space that may have been missed by previous studies (at the expense of potentially sampling structure−property combinations that are not physically realizable).[62]

In brief, our approach involved generating a library of 600 000 porous crystals, represented by configurations of LJ spheres within a unit cell. Six properties were then evaluated for each pseudomaterial: methane loading (at both 35 and 65 bar), void fraction, volumetric surface area, average ε value, average σ value, and number density. We then generated 2D projections of the property space, where the data were grouped into bins that were colored by some third property; the result is a heatmap showing various structure−property relationships in three dimensions.

Received: May 4, 2018
Accepted: July 7, 2018
Published: July 8, 2018

## METHODS

Lennard-Jones Potential. Our pseudomaterials were constructed using LJ spheres, meant to represent different chemical species or moieties, to create structures for use in Grand Canonical Monte Carlo (GCMC) simulations of methane physisorption. The LJ potential is commonly used in computational studies of physisorption in porous materials and has been experimentally validated numerous times.[44,47,49,63] There are well-documented limitations of the LJ potential in the context of adsorption, such as chemisorption or physisorption, where the binding is very strong (as is the case for certain gases and open metal sites). It may stand that even higher methane capacities may be attainable in systems that rely on chemisorption or take advantage of other physical phenomena not captured by LJ interactions.

Generating Pseudomaterials. Pseudomaterials were generated by randomly positioning LJ spheres, which we refer to as pseudoatoms, within a randomly sized unit cell (see Figure 1).

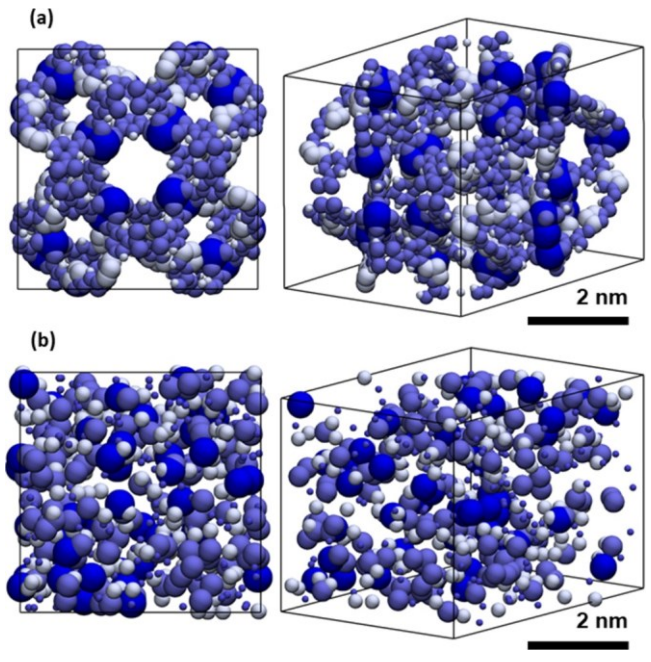


Figure 1. Renderings of (a) a synthesizable MOF, NU-125, and (b) a randomly generated configuration of LJ spheres, or pseudomaterial.

The unit cell dimensions were bounded between 25.6 and 51.2 Å in each of the crystallographic directions (with the lower bound twice the cutoff length used for gas−gas and gas−crystal interactions: 12.8 Å) (Table 1). The number of LJ spheres within a unit cell was bounded between $1.49 \times 10^{-5}$ and 0.02122 atoms/Å$^3$, where the lower boundary ensured that each unit cell contained at least two atom sites and the upper boundary corresponded to 10% of the number density of iron.

Table 1. Pseudomaterial Generation Steps and Related Parameter Ranges

| | pseudomaterial generation step | parameter range |
|---|---|---|
| 1 | select lattice constants | 25.6−51.2 Å |
| 2 | select number density | $1.49 \times 10^5$ to 0.02122 atoms/Å$^3$ |
| 3 | position pseudoatom sites | N/A |
| 4 | select four sets of LJ parameters (one for each pseudoatom type) | σ: 1.052−6.549 Å; ε: 1.258−513.264 K |
| 5 | assign each pseudoatom site to one of the four pseudoatom types | N/A |

Pseudoatom types were defined by their LJ parameters: σ, the van der Waals radius, and ε, the potential well depth. Values for σ were bounded between 1.052 and 6.549 Å and values for ε between 1.258 and 513.264 K. This range of LJ parameters was based on the Universal Force Field (UFF),[64] where σ/ε values were allowed to be 50% lower or greater, respectively, than the minimum and maximum values present in the UFF. Whereas a particular pseudomaterial's unit cell may contain hundreds of pseudoatoms depending


DOI: 10.1021/acs.jpclett.8b01421
J. Phys. Chem. Lett. 2018, 9, 4275−4281

upon the randomly selected number density, the number of pseudoatom types was limited to four in all pseudomaterials. In this study, we generated a library of 600 000 pseudomaterials: two independent sets of 300 000 materials for each methane loading pressure.

Simulating Properties. After each pseudomaterial was created, its atomistically detailed structure was used in a GCMC simulation to calculate methane adsorption at 298 K and either 35 or 65 bar. These pressures were chosen primarily because the community has converged on these two pressures as benchmarks for high-pressure methane storage. It may interest the reader to know that 35 bar is the typical pressure of U.S. interstate natural gas pipelines, and 65 bar is the upper limit achievable with inexpensive two-stage compressors.[51] Pseudomaterials were treated as rigid structures, where pseudoatom site positions were held constant throughout the simulation. Void fractions were calculated using a Widom insertion method[65] using a helium probe ($\sigma = 2.96$ Å). Volumetric surface areas were calculated in a Monte Carlo search, rolling a nitrogen probe ($\sigma = 3.31$ Å) over the surface of the unit cell. All of these properties were calculated using a simulation software package for adsorption in nanoporous materials called RASPA.[65]

As expected, the more pseudomaterials we generated, the larger the volume of the structure−property space we sampled (see Figure 2). However, we also expected that at a certain size the library would be sufficiently large such that no new features would be observed with the addition of new pseudomaterials. Figure 2 demonstrates that, when generated at random using our approach discussed in the Methods section, several hundred thousand pseudomaterials were needed before the addition of new materials became redundant. It was not until tens of thousands of materials had been sampled (Figure 2c) that the upper limits of methane capacity were observed. Also, certain combinations of properties were much more likely than others. For example, we found that the randomly generated pseudomaterials most commonly had void fractions between 0.5 and 0.9, as can be seen most clearly in Figure 2d.

Once our library was sufficiently large, we were able to observe the distribution of materials across various 2D projections (see Figure 3). We observed that the highest methane loadings (regardless of pressure) occurred at void

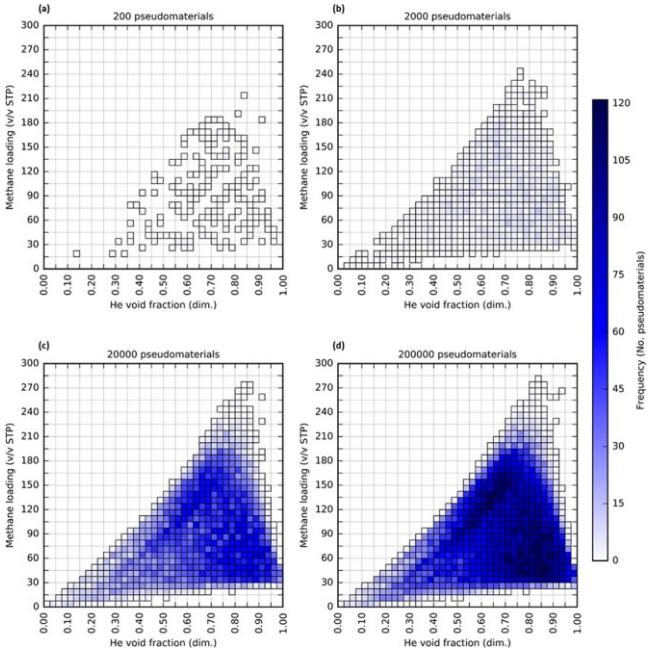


Figure 2. 2D histograms for samples of (a) 200, (b) 2000, (c) 20 000, and (d) 200 000 pseudomaterials from a library of 300 000 pseudomaterials. Plots show projections of the structure−property space in methane loading (at 35 bar) with respect to helium void fraction and are colored by the number of pseudomaterials in each of 40 × 40 equally sized bins.

fractions between 0.7 and 0.9 and at volumetric surface areas exceeding 3150 $m^2/cm^3$. This is similar to what has been reported previously by others for MOFs.[44] We found that our pseudomaterials most commonly had volumetric surface areas between 1350 and 3600 $m^2/cm^3$, as shown in Figure 3c,f. (Note that panels c and f of Figure 3 are nearly identical, as expected, because the properties displayed do not depend on pressure.) We also found that the highest surface areas occurred in a void fraction range of 0.7 to 0.95. Not surprisingly, a larger distribution of pseudomaterials occupied the high methane loading domain in the 65 bar library. Most notably, we observed the highest volumetric surface area pseudomaterials associated with the highest methane loadings. It is important to point out that these observations are based on the simulated interactions of methane with an atomistically detailed porous crystal structure and that the influence of mean geometric properties such as void fraction and surface area are only being inferred in a later data analysis stage (as opposed to predicting methane adsorption directly from void fractions and surface areas).



DOI: 10.1021/acs.jpclett.8b01421
J. Phys. Chem. Lett. 2018, 9, 4275−4281

Two critical parameters of this LJ-based model are, of course, the influence of the ε and σ values on methane loading. Because each pseudomaterial contained a range of both, we used average values in plotting structure−property relationships. The average ε value in a pseudomaterial provided a measure of the availability of strong (or weak) binding sites in the pseudomaterial. In Figure 4, we show the relationship between this average ε value and void fraction, surface area, and methane loading at both pressures. Figure 4a,c shows that, at void fraction values above ~0.3, the presence of strong binding sites (here represented by high average ε values) was necessary to maximize methane loading. Also, median average ε values typically corresponded to median methane loading;

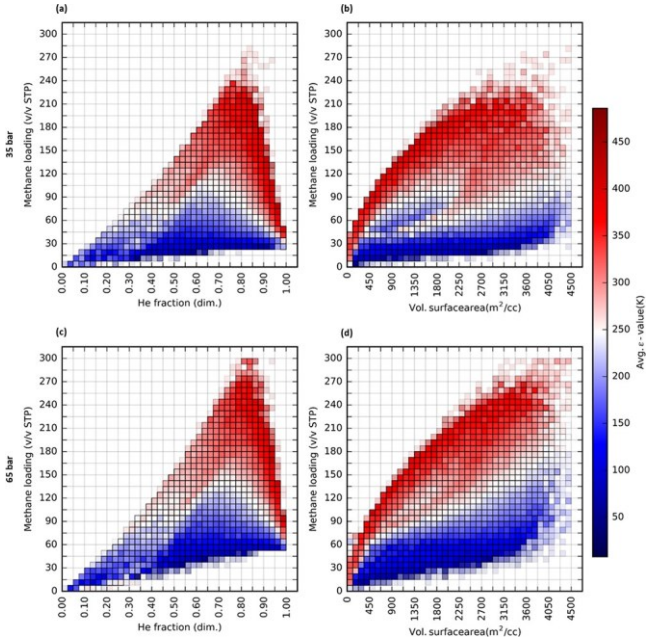


Figure 4. 2D projections of the structure−property space colored by average ε value for all pseudomaterials within each 40 × 40 bin. Projections shown here: methane capacity with respect to void fraction (a,c) and methane capacity with respect to surface area (b,d). The top row of plots corresponds to an operating pressure (for methane adsorption simulations) of 35 bar (a,b) with results at 65 bar below (c,d).

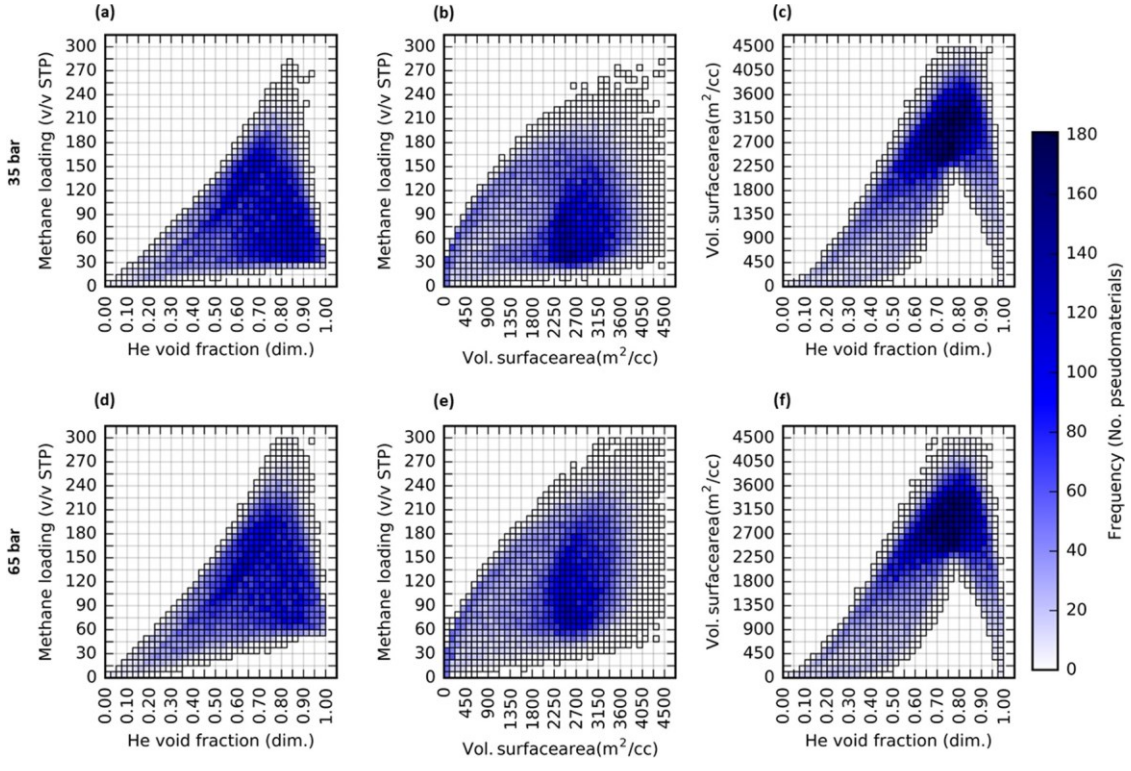


Figure 3. 2D histograms for the full library of 300 000 pseudomaterials. Plots show different projections of the structure−property space colored by number of pseudomaterials in each of the 40 × 40 equally sized bins. Projections shown here: methane capacity with respect to void fraction (a,d), methane capacity with respect to surface area (b,e), and surface area with respect to void fraction (c,f). The top row of plots corresponds to an operating pressure (for methane adsorption simulations) of 35 bar (a−c) with results at 65 bar below (d−f).


DOI: 10.1021/acs.jpclett.8b01421
J. Phys. Chem. Lett. 2018, 9, 4278−4282

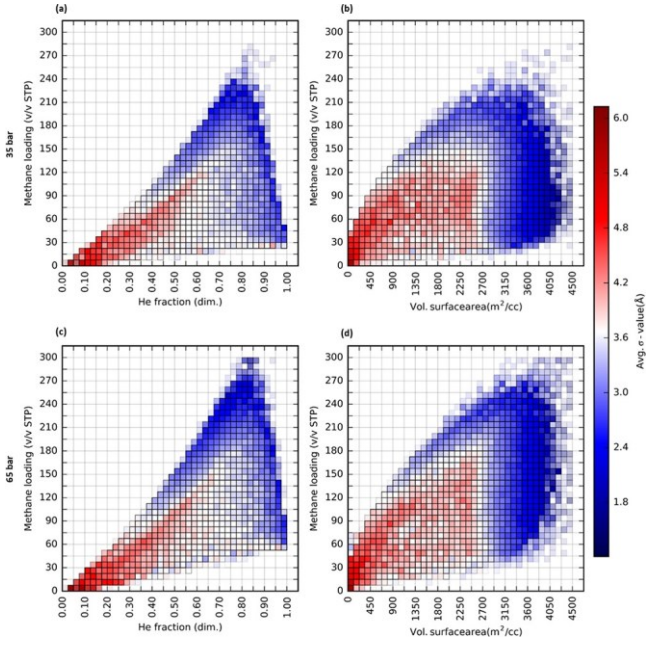


Figure 5. 2D projections of the structure−property space colored by average σ value for all pseudomaterials within each 40 × 40 bin. Projections shown here: methane capacity with respect to void fraction (a,c) and methane capacity with respect to surface area (b,d). The top row of plots corresponds to an operating pressure (for methane adsorption simulations) of 35 bar (a,b) with results at 65 bar below (c,d).

however, sometimes high surface area pseudomaterials were able to store more methane than ones with higher ε values but lower surface areas (see Figure 4b,d). At 65 bar, we saw higher methane loadings out of lower average ε-value pseudomaterials; this demonstrated, as one might expect, that increasing the pressure decreased the need for strong binding sites given the same porosity.

We also looked at similar relationships considering the average σ values (see Figure 5). Interestingly, we observed that both the highest methane loadings and highest surface areas occurred when the average atom/moiety sizes (represented here by average σ values) were the smallest. Conversely, large atom sites/moieties corresponded with below-average surface areas and methane loadings. The very highest methane loadings were not achievable above a certain average σ value; however, below this domain, average σ values were constant at constant surface areas. These low to medium-high methane loadings were much more strongly influenced by the availability of strong binding sites than by the average pseudoatom size.

Finally, we considered the effect of number density on methane loadings. First, we divided our two 300 000 material libraries into low, medium, and high number density groups. Then, we colored by methane loading and plotted average σ value with respect to average ε values (see Figure 6). We found that the highest methane loadings were observed among medium-to-high number density pseudomaterials. The highest methane loadings were observed in those pseudomaterials with higher-than-average ε values and lower-than-average σ values. With high number densities, methane loading clearly depended on both σ and ε (see Figure 6d,g). However, at lower number densities, methane loading was independent of σ (see Figure 6a,e).

Figure 7 shows pseudomaterial structures from disparate regions of the structure−property space. In low methane loading pseudomaterials (I, III, and V), we see fewer strong binding sites than in higher methane loading pseudomaterials (II and IV). Pseudomaterial IV had a lower average σ value than pseudomaterial II, which contributed to its higher methane loading. Pseudomaterial IV was substantially less porous than pseudomaterial V, which also lacked a dense network of strong binding sites. When examining these structures, we continued to see that strong binding sites (high average ε values) as well as relatively low σ values and an appropriately high level of porosity made the best methane adsorbents.

In conclusion, we have used a novel approach to examine structure−property relationships of physisorption in porous materials, namely, by generating and screening libraries of "pseudomaterials," periodic configurations of LJ spheres, each representing a particular chemical species or moiety. The use of these more abstract structures allowed us to flexibly explore the space of porous materials and avoid potential limitations and challenges in generating structures using chemical building blocks and design rules.

We generated two libraries of 300 000 pseudomaterials and for each material simulated methane capacity at 35 and 65 bar. We then compared the methane capacities for each material with their helium void fraction, volumetric surface area, average σ values, average ε values, and number density. We found the randomly generated pseudomaterials most commonly had void fractions between 0.5 and 0.9 and volumetric surface areas between 1350 and 3600 $m^2/cm^3$. The highest methane loadings occurred at void fractions between 0.5 and 0.9 and at surface areas exceeding 3150 $m^2/cm^3$. Strong binding sites were necessary for higher methane loadings, as



DOI: 10.1021/acs.jpclett.8b01421
J. Phys. Chem. Lett. 2018, 9, 4275−4281

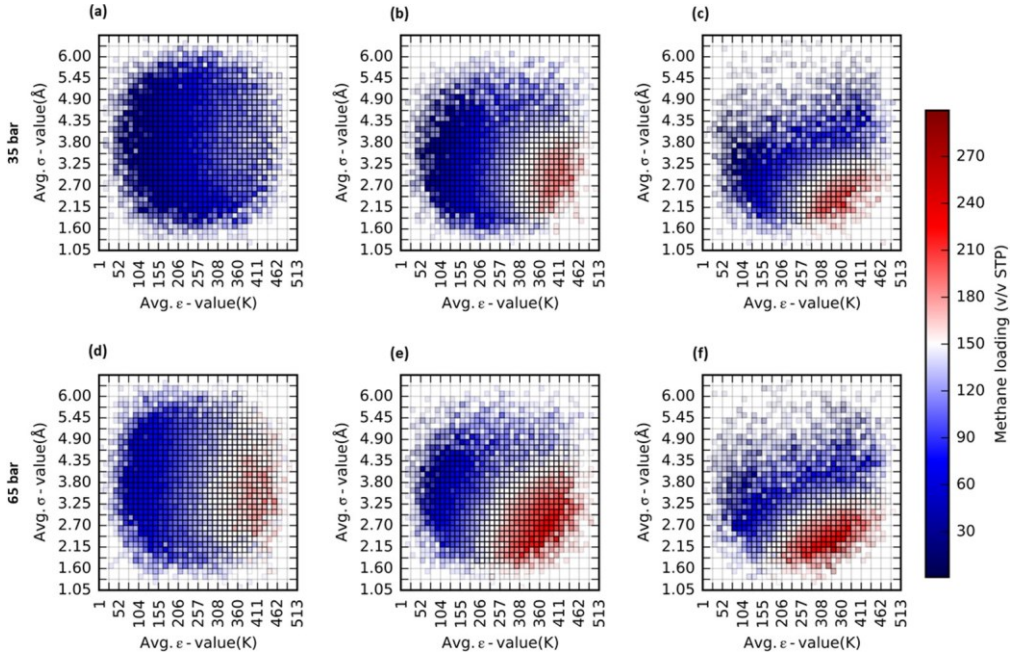


Figure 6. 2D projections of the structure−property space in average σ value with respect to average ε value colored by methane capacity. The plots represent subsets of the 300 000 pseudomaterial library containing low (a,d), medium (b,e), and high (c,f) number density pseudomaterials. The top row of plots corresponds to an operating pressure (for methane adsorption simulations) of 35 bar (a−c) with results at 65 bar below (d−f).

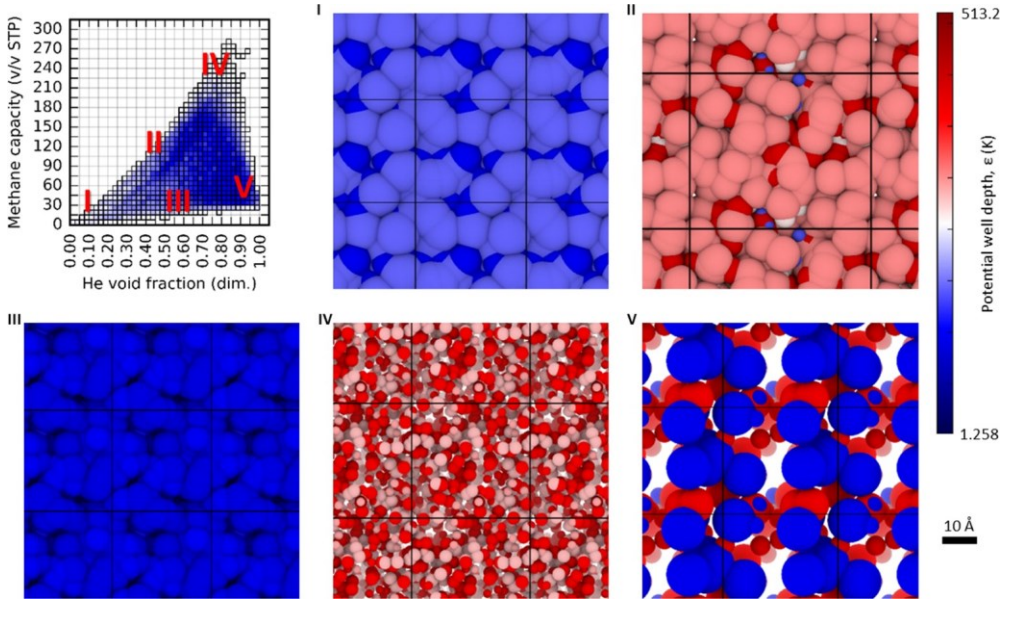


Figure 7. Renderings of pseudomaterials from different regions of the structure−property space. The plot (top left) shows where each pseudomaterial is located with respect to void fraction and methane loading: (I) low void fraction and low methane loading, (II) medium low void fraction and medium methane loading, (III) medium void fraction and low methane loading, (IV) medium high void fraction and high methane loading, and (V) high void fraction and low methane loading.

were smaller atoms/moieties and medium-to-high number densities.

Finally, we looked at several individual structures from different regions of our structure−property space. We continued to see that strong binding sites (high average ε values) as well as relatively low σ values and an appropriately high level of porosity made the best methane adsorbents. It is important to note that in this broad and abstract search we did not find candidate materials that meet the DOE's methane storage targets, despite the relaxation of many constraints on realism. Fundamentally, there appears to be a trade-off between strong binding and volume, and maximum methane capacity under these conditions appears just below these targets.



DOI: 10.1021/acs.jpclett.8b01421
J. Phys. Chem. Lett. 2018, 9, 4275−4281

We believe this pseudomaterials approach offers useful information for efficiently creating structure−property maps for gas adsorption that experimental researchers who seek to design new adsorbents can use not only for methane storage but also for a broad range of gas adsorption applications.

## ASSOCIATED CONTENT

* Supporting Information

The Supporting Information is available free of charge on the ACS Publications website at DOI: 10.1021/acs.jpclett.8b01421.

(S1) Additional simulation details including force-field parameters. (S2) Additional structure−property plots shown with extended ranges. (PDF)

## AUTHOR INFORMATION

Corresponding Author

*E-mail: wilmer@pitt.edu.

ORCID

Christopher E. Wilmer: 0000-0002-7440-5727

Notes

The authors declare no competing financial interest.

## ACKNOWLEDGMENTS

A.R.K. and C.E.W. gratefully acknowledge support from the National Science Foundation (NSF award CBET-1653375). They also acknowledge both the Swanson School of Engineering and the Center for Research Computing (CRC) at the University of Pittsburgh for initial financial support and for providing computational resources, respectively.

## REFERENCES

(1) Yaghi, O. M.; Li, H. Hydrothermal Synthesis of a Metal-Organic Framework Containing Large Rectangular Channels. J. Am. Chem. Soc. 1995, 117 (41), 10401−10402.

(2) Janiak, C. Engineering Coordination Polymers towards Applications. Dalton Trans. 2003, 0 (14), 2781−2804.

(3) Meek, S. T.; Greathouse, J. A.; Allendorf, M. D. Metal-Organic Frameworks: A Rapidly Growing Class of Versatile Nanoporous Materials. Adv. Mater. 2011, 23 (2), 249−267.

(4) Rowsell, J. L. C.; Yaghi, O. M. Metal-Organic Frameworks: A New Class of Porous Materials. Microporous Mesoporous Mater. 2004, 73 (1−2), 3−14.

(5) Mueller, U.; Schubert, M.; Teich, F.; Puetter, H.; Schierle-Arndt, K.; Pastre, J. Metal −Organic Frameworks—Prospective Industrial Applications. J. Mater. Chem. 2006, 16 (7), 626−636.

(6) James, S. Metal-Organic Frameworks. Chem. Soc. Rev. 2003, 32
(5), 276−288.

(7) Sanchez, C.; Julian, B.; Belleville, P.; Popall, M. Applications of Hybrid Organic−Inorganic Nanocomposites. J. Mater. Chem. 2005, 15 (35−36), 3559−3592.

(8) Zhao, D.; Timmons, D. J.; Yuan, D.; Zhou, H.-C. Tuning the Topology and Functionality of Metal−Organic Frameworks by Ligand Design. Acc. Chem. Res. 2011, 44 (2), 123−133.

(9) Bai, Y.; Dou, Y.; Xie, L.-H.; Rutledge, W.; Li, J.-R.; Zhou, H.-C. Zr-Based Metal−Organic Frameworks: Design, Synthesis, Structure, and Applications. Chem. Soc. Rev. 2016, 45 (8), 2327−2367.

(10) Rowsell, J. L. C.; Yaghi, O. M. Strategies for Hydrogen Storage in Metal−Organic Frameworks. Angew. Chem., Int. Ed. 2005, 44 (30), 4670−4679.

(11) Getman, R. B.; Bae, Y.-S.; Wilmer, C. E.; Snurr, R. Q. Review and Analysis of Molecular Simulations of Methane, Hydrogen, and Acetylene Storage in Metal−Organic Frameworks. Chem. Rev. 2012, 112 (2), 703−723.

(12) Liu, C.; Li, F.; Ma, L.-P.; Cheng, H.-M. Advanced Materials for Energy Storage. Adv. Mater. 2010, 22 (8), E28−E62.

(13) Ma, S.; Zhou, H.-C. Gas Storage in Porous Metal−Organic Frameworks for Clean Energy Applications. Chem. Commun. 2010, 46 (1), 44−53.

(14) Li, H.; Eddaoudi, M.; O′Keeffe, M.; Yaghi, O. M. Design and Synthesis of an Exceptionally Stable and Highly Porous MetalOrganic Framework. Nature 1999, 402 (6759), 276−279.

(15) Wilmer, C. E.; Farha, O. K.; Yildirim, T.; Eryazici, I.; Krungleviciute, V.; Sarjeant, A. A.; Snurr, R. Q.; Hupp, J. T. GramScale, High-Yield Synthesis of a Robust Metal−Organic Framework for Storing Methane and Other Gases. Energy Environ. Sci. 2013, 6 (4), 1158−1163.

(16) Bobbitt, N. S.; Chen, J.; Snurr, R. Q. High-Throughput Screening of Metal−Organic Frameworks for Hydrogen Storage at Cryogenic Temperature. J. Phys. Chem. C 2016, 120 (48), 27328−27341.

(17) Rosi, N. L.; Eckert, J.; Eddaoudi, M.; Vodak, D. T.; Kim, J.; O′Keeffe, M.; Yaghi, O. M. Hydrogen Storage in Microporous MetalOrganic Frameworks. Science 2003, 300 (5622), 1127−1129.

(18) Furukawa, H.; Cordova, K. E.; O′Keeffe, M.; Yaghi, O. M. The Chemistry and Applications of Metal-Organic Frameworks. Science 2013, 341 (6149), 1230444.

(19) Li, J.-R.; Kuppler, R. J.; Zhou, H.-C. Selective Gas Adsorption and Separation in Metal-Organic Frameworks. Chem. Soc. Rev. 2009, 38 (5), 1477−1504.

(20) Seo, J. S.; Whang, D.; Lee, H.; Jun, S. I.; Oh, J.; Jeon, Y. J.; Kim, K. A Homochiral Metal−Organic Porous Material for Enantioselective Separation and Catalysis. Nature 2000, 404 (6781), 982−986. (21) Li, J.-R.; Sculley, J.; Zhou, H.-C.



DOI: 10.1021/acs.jpclett.8b01421
J. Phys. Chem. Lett. 2018, 9, 4275−4281

Metal−Organic Frameworks for Separations. Chem. Rev. 2012, 112 (2), 869−932.
(22) Chae, H. K.; Siberio-Perez, D. Y.; Kim, J.; Go, Y.; Eddaoudi, M.; Matzger, A. J.; O'Keeffe, M.; Yaghi, O. M. A Route to High Surface Area, Porosity and Inclusion of Large Molecules in Crystals. Nature 2004, 427 (6974), 523−527.
(23) Chen, X.; Plonka, A. M.; Banerjee, D.; Krishna, R.; Schaef, H. T.; Ghose, S.; Thallapally, P. K.; Parise, J. B. Direct Observation of Xe and Kr Adsorption in a Xe-Selective Microporous Metal−Organic Framework. J. Am. Chem. Soc. 2015, 137 (22), 7007−7010.
(24) Rodenas, T.; Luz, I.; Prieto, G.; Seoane, B.; Miro, H.; Corma, A.; Kapteijn, F.; Llabres i Xamena, F. X.; Gascon, J. Metal−Organic Framework Nanosheets in Polymer Composite Materials for Gas Separation. Nat. Mater. 2015, 14 (1), 48−55.
(25) Sikora, B. J.; Wilmer, C. E.; Greenfield, M. L.; Snurr, R. Q. Thermodynamic Analysis of Xe/Kr Selectivity in over 137,000 Hypothetical Metal−Organic Frameworks. Chem. Sci. 2012, 3 (7), 2217−2223.
(26) Bae, Y.-S.; Snurr, R. Q. Development and Evaluation of Porous Materials for Carbon Dioxide Separation and Capture. Angew. Chem., Int. Ed. 2011, 50 (49), 11586−11596.
(27) Liu, J.; Chen, L.; Cui, H.; Zhang, J.; Zhang, L.; Su, C.-Y. Applications of Metal−Organic Frameworks in Heterogeneous Supramolecular Catalysis. Chem. Soc. Rev. 2014, 43 (16), 6011−6061.
(28) Ma, L.; Abney, C.; Lin, W. Enantioselective Catalysis with Homochiral Metal-Organic Frameworks. Chem. Soc. Rev. 2009, 38 (5), 1248−1256.
(29) Corma, A.; García, H.; Llabres i Xamena, F. X. Engineering Metal Organic Frameworks for Heterogeneous Catalysis. Chem. Rev. 2010, 110 (8), 4606−4655.
(30) Lee, J.; Farha, O. K.; Roberts, J.; Scheidt, K. A.; Nguyen, S. T.; Hupp, J. T. Metal−Organic Framework Materials as Catalysts. Chem. Soc. Rev. 2009, 38 (5), 1450−1459.
(31) Taguchi, A.; Schüth, F. Ordered Mesoporous Materials in Catalysis. Microporous Mesoporous Mater. 2005, 77 (1), 1−45.
(32) Davis, M. E. Ordered Porous Materials for Emerging Applications. Nature 2002, 417 (6891), 813−821.
(33) Chen, B.; Xiang, S.; Qian, G. Metal−Organic Frameworks with Functional Pores for Recognition of Small Molecules. Acc. Chem. Res. 2010, 43 (8), 1115−1124.
(34) Hu, Z.; Deibert, B. J.; Li, J. Luminescent Metal−Organic Frameworks for Chemical Sensing and Explosive Detection. Chem. Soc. Rev. 2014, 43 (16), 5815−5840.
(35) Kreno, L. E.; Leong, K.; Farha, O. K.; Allendorf, M.; Van Duyne, R. P.; Hupp, J. T. Metal−Organic Framework Materials as Chemical Sensors. Chem. Rev. 2012, 112 (2), 1105−1125.
(36) Jiang, H.-L.; Tatsu, Y.; Lu, Z.-H.; Xu, Q. Non-, Micro-, and Mesoporous Metal−Organic Framework Isomers: Reversible Transformation, Fluorescence Sensing, and Large Molecule Separation. J. Am. Chem. Soc. 2010, 132 (16), 5586−5587.
(37) Wang, L.; Han, Y.; Feng, X.; Zhou, J.; Qi, P.; Wang, B. Metal− Organic Frameworks for Energy Storage: Batteries and Supercapacitors. Coord. Chem. Rev. 2016, 307, 361−381.
(38) Ockwig, N. W.; Delgado-Friedrichs, O.; O'Keeffe, M.; Yaghi, O. M. Reticular Chemistry: Occurrence and Taxonomy of Nets and Grammar for the Design of Frameworks. Acc. Chem. Res. 2005, 38 (3), 176−182.
(39) Martin, R. L.; Simon, C. M.; Smit, B.; Haranczyk, M. In Silico Design of Porous Polymer Networks: High-Throughput Screening for Methane Storage Materials. J. Am. Chem. Soc. 2014, 136 (13), 5006− 5022.
(40) Colon, Y. J.; Snurr, R. Q. High-Throughput Computational Screening of Metal−Organic Frameworks. Chem. Soc. Rev. 2014, 43 (16), 5735−5749.
(41) Chung, Y. G.; Camp, J.; Haranczyk, M.; Sikora, B. J.; Bury, W.; Krungleviciute, V.; Yildirim, T.; Farha, O. K.; Sholl, D. S.; Snurr, R. Q. Computation-Ready, Experimental Metal−Organic Frameworks: A Tool To Enable High-Throughput Screening of Nanoporous Crystals. Chem. Mater. 2014, 26 (21), 6185−6192.
(42) Curtarolo, S.; Hart, G. L. W.; Nardelli, M. B.; Mingo, N.; Sanvito, S.; Levy, O. The High-Throughput Highway to Computational Materials Design. Nat. Mater. 2013, 12 (3), 191−201.
(43) Simon, C. M.; Kim, J.; Gomez-Gualdron, D. A.; Camp, J. S.; Chung, Y. G.; Martin, R. L.; Mercado, R.; Deem, M. W.; Gunter, D.; Haranczyk, M.; et al. The Materials Genome in Action: Identifying the Performance Limits for Methane Storage. Energy Environ. Sci. 2015, 8 (4), 1190−1199.
(44) Wilmer, C. E.; Farha, O. K.; Bae, Y.-S.; Hupp, J. T.; Snurr, R. Q. Structure−Property Relationships of Porous Materials for Carbon Dioxide Separation and Capture. Energy Environ. Sci. 2012, 5 (12), 9849−9856.
(45) Meador, M. A. B.; Capadona, L. A.; McCorkle, L.; Papadopoulos, D. S.; Leventis, N. Structure−Property Relationships in Porous 3D Nanostructures as a Function of Preparation Conditions: Isocyanate Cross-Linked Silica Aerogels. Chem. Mater. 2007, 19 (9), 2247−2260.
(46) Bonakala, S.; Balasubramanian, S. Structure−Property Relationships in Amorphous Microporous Polymers. J. Phys. Chem. B 2016, 120 (3), 557−565.
(47) Wilmer, C. E.; Leaf, M.; Lee, C. Y.; Farha, O. K.; Hauser, B. G.; Hupp, J. T.; Snurr, R. Q. Large-Scale Screening of Hypothetical Metal−Organic Frameworks. Nat. Chem. 2012, 4 (2), 83−89.
(48) Poloni, R.; Lee, K.; Berger, R. F.; Smit, B.; Neaton, J. B. Understanding Trends in CO2 Adsorption in Metal−Organic Frameworks with Open-Metal Sites. J. Phys. Chem. Lett. 2014, 5 (5), 861−865.
(49) Li, S.; Chung, Y. G.; Snurr, R. Q. High-Throughput Screening of Metal−Organic Frameworks for CO2 Capture in the Presence of Water. Langmuir 2016, 32 (40), 10368−10376.
(50) Haldoupis, E.; Nair, S.; Sholl, D. S. Pore Size Analysis of > 250 000 Hypothetical Zeolites. Phys. Chem. Chem. Phys. 2011, 13 (11), 5053−5060.
(51) Peng, Y.; Krungleviciute, V.; Eryazici, I.; Hupp, J. T.; Farha, O. K.; Yildirim, T. Methane Storage in Metal−Organic Frameworks: Current Records, Surprise Findings, and Challenges. J. Am. Chem. Soc. 2013, 135 (32), 11887−11894.
(52) Mason, J. A.; Veenstra, M.; Long, J. R. Evaluating Metal− Organic Frameworks for Natural Gas Storage. Chem. Sci. 2014, 5 (1), 32−51.



DOI: 10.1021/acs.jpclett.8b01421
J. Phys. Chem. Lett. 2018, 9, 4275−4281

(53) Gandara, F.; Furukawa, H.; Lee, S.; Yaghi, O. M. High Methané Storage Capacity in Aluminum Metal−Organic Frameworks. J. Am. Chem. Soc. 2014, 136 (14), 5271−5274.
(54) Pophale, R.; Cheeseman, P. A.; Deem, M. W. A Database of New Zeolite-like Materials. Phys. Chem. Chem. Phys. 2011, 13 (27), 12407−12412.
(55) Deem, M. W.; Pophale, R.; Cheeseman, P. A.; Earl, D. J. Computational Discovery of New Zeolite-Like Materials. J. Phys. Chem. C 2009, 113 (51), 21353−21360.
(56) Lin, L.-C.; Berger, A. H.; Martin, R. L.; Kim, J.; Swisher, J. A.; Jariwala, K.; Rycroft, C. H.; Bhown, A. S.; Deem, M. W.; Haranczyk, M.; et al. In Silico Screening of Carbon-Capture Materials. Nat. Mater. 2012, 11 (7), 633−641.
(57) Bracco, S.; Piga, D.; Bassanetti, I.; Perego, J.; Comotti, A.; Sozzani, P. Porous 3D Polymers for High Pressure Methane Storage and Carbon Dioxide Capture. J. Mater. Chem. A 2017, 5 (21), 10328−10337.
(58) Tong, W.; Lv, Y.; Svec, F. Advantage of Nanoporous StyreneBased Monolithic Structure over Beads When Applied for Methane Storage. Appl. Energy 2016, 183, 1520−1527.
(59) Duan, J.; Jin, W.; Krishna, R. Natural Gas Purification Using a Porous Coordination Polymer with Water and Chemical Stability. Inorg. Chem. 2015, 54 (9), 4279−4284.
(60) Sun, L.-B.; Li, A.-G.; Liu, X.-D.; Liu, X.-Q.; Feng, D.; Lu, W.; Yuan, D.; Zhou, H.-C. Facile Fabrication of Cost-Effective Porous Polymer Networks for Highly Selective CO2 Capture. J. Mater. Chem. A 2015, 3 (7), 3252−3256.
(61) Wood, C. D.; Tan, B.; Trewin, A.; Su, F.; Rosseinsky, M. J.; Bradshaw, D.; Sun, Y.; Zhou, L.; Cooper, A. I. Microporous Organic Polymers for Methane Storage. Adv. Mater. 2008, 20 (10), 1916− 1921.
(62) Kaija, A. R.; Wilmer, C. E. Efficiently Mapping Structure− Property Relationships of Gas Adsorption in Porous Materials: Application to Xe Adsorption. Faraday Discuss. 2017, 201 (0), 221− 232.
(63) Frost, H.; Snurr, R. Q. Design Requirements for Metal-Organic Frameworks as Hydrogen Storage Materials. J. Phys. Chem. C 2007, 111 (50), 18794−18803.
(64) Rappe, A. K.; Casewit, C. J.; Colwell, K. S.; Goddard, W. A., III; Skiff, W. M. UFF, a Full Periodic Table Force Field for Molecular Mechanics and Molecular Dynamics Simulations. J. Am. Chem. Soc. 1992, 114 (25), 10024−10035.
(65) Dubbeldam, D.; Calero, S.; Ellis, D. E.; Snurr, R. Q. RASPA: Molecular Simulation Software for Adsorption and Diffusion in Flexible Nanoporous Materials. Mol. Simul. 2016, 42 (2), 81−101.



DOI: 10.1021/acs.jpclett.8b01421
J. Phys. Chem. Lett. 2018, 9, 4275−4281